Multi-Objective Optimisation of a 1-kW Wireless IPT Systems for Charging of Electric vehicles

Soumya Bandyopadhyay*,Venugopal Prasanth*, Pavol Bauer* and J.A. Ferreira*
*Dept. Electrical Sustainable Energy, DCE&S group
TU Delft, Meklweg 04, 2628 CD, Delft, the Netherlands
Email: s.bandyopadhyay@tudelft.nl, v.prasanth@tudelft.nl, p.bauer@tudelft.nl and j.a.ferreira@tudelft.nl

***Abstract*—Inductive power transfer (IPT) systems for on-road dynamic charging of electric vehicles (EVs) must employ tracks with minimal copper and ferrite core material for improving coupling and field shaping without sacrificing on power transfer efficiency across the air gap. This paper details the multi-objective optimisation of IPT coil systems with respect to efficiency of power transfer (η) , material weight or cost (w), and area-power density (α) as required in EV applications. A combination of detailed analytical calculations and experimentally verified 3D finite element models is used to analyse performance of IPT systems with polarized coupler topology [referred to as double D(DD) coils], I-shaped ferrite cores for field shaping and aluminium plates to reduce stray or leakage magnetic fields. An multi-objective pareto optimisation using Particle Swarm algorithm of a scaled 1kW prototype system with a 15 cm airgap is presented.**

***Index Terms* - Electric vehicles, Finite element modelling, Inductive power transfer (IPT), Multi-objective optimisation, Particle swarm optimisation**

I. Introduction

Inductive charging of electric vehicles and hybrid electric vehicles (EV/HEV) have become increasingly popular in recent years. Inductive power transfer systems (IPT) for recharging of traction batteries has been proposed as an alternative to conventional battery charging systems. Due to the absence of electrical or mechanical contacts as seen in conductive charging, IPT systems are reliable and maintenance free. Due to these advantages IPT systems are used in a wide range of applications [1], [2], [3].

The state of the art in mobility based inductive power transfer system is the concept of Roadway Powered Electric Vehicles (RPEVs) [4], [5], [6]. Futuristic vision of road transport involves transforming the highways into energy hubs by laying coils on/underneath the roads and transferring power to the moving/stationary vehicles as on demand. Since power is transferred real time to the drive train for propelling the EV, this technique can also be referred to as powering while driving [7]. Due to significant simplification of the charging process and electric insulation provided by a contact-less system, IPT brings forward the convenience and safety for the users and therefore can be a crucial factor for a further increase in the popularity of EVs.

Designing a lumped IPT system for the use in an EV/HEV, a number of constraints like space of the pick-up coil in the underfloor of the vehicle and the allowable weight and cost of the components used in both the primary and the secondary exists. The power transfer efficiency should be high as possible for simple thermal management of the system. In addition to that, another design constraint arises from the limitation of the magnetic stray field in the vicinity of the IPT coils by well-defined International Commission on Non-Ionizing Radiation Protection (ICNIRP) standards [8].

The magnetic design of the transmission coils is of paramount importance in order to satisfy the mutually conflicting targets like efficiency, area-related power density and weight of copper and ferrite materials. In literature, it is shown that a Figure of Merit (FOM) = kQ given by the product of the magnetic coupling of the IPT coils and the inductor quality factor limits the maximum efficiency of power transfer [9]. To achieve high power transfer efficiency, large coils can be used at the cost of power density and charge pad weight. A high power density and light charge pad can be similarly designed at the cost of low power transfer efficiency and possibly thermal problems.In this paper, it is shown how the three performance indices efficiency (η), power density (α) and material weight (w) are related and that a trade-off is encountered in the design optimisation of charge pad design in IPT systems, similar to other power electronic systems and in design of electric machines [10].

Nowadays, with increased computer speeds, accurate Finite Element (FE) charge-pad models combined with multi-objective evolutionary algorithms are be used to design high performance IPT systems The goal of this paper is to present a systematic multi-objective framework for design optimisation of 1kW, 85 kHz IPT systems to realise the trade off between targets and to draw general design guidelines based on that. A multi-objective PSO algorithm combined with 3D FE charge-pad models is used to optimise the IPT system to generate Pareto Optimal fronts [11], [12]. The coil topology used in design of the IPT systems is the polarized coupler topology or also known as the DD coils, mainly due to their high tolerance to misalignment which is necessary for dynamic charging of EVs [13]. To improve coupling and proper field shaping I-shaped ferrite bars are used. To reduce stray or leakage fields around the IPT coils aluminium sheets in both primary and secondary charge-pads are used.

This paper is structured in five sections. In Section II, a series-series compensated IPT charging system is presented with detailed analysis of the FOMs of the system along with

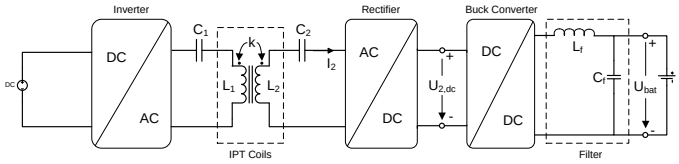

Fig. 1. Schematic representation of a 1-kW Prototype IPT system

TABLE I
SPECIFICATIONS OF THE PROTOTYPE IPT SYSTEM

Parameters	Value	Description
f	85 kHz	Frequency of Operation
P_2	1000 W	Power Output
δ	0.15 m	Air-Gap
U_{bat}	40 V	Battery Voltage
$U_{2,dc}$	100 V	Receiver side dc-link voltage
W_{coil}	0.2 m	Maximum Coil Width
L_{coil}	0.22 m	Maximum Coil Length

the layout of the charge-pad. The FE modelling procedure to extract IPT performance data is discussed in Section III. The multi-objective $\eta-\alpha-w$ Optimisation framework is developed in the next section along with detailed optimisation results highlighting the trade off between efficiency, power density and weight of an example IPT system. The measurement results are presented in Section V to validate the design procedure and to demonstrate the accuracy of the FE models. Concluding remarks are given in Section VI.

II. IPT EV CHARGING SYSTEM

A generic lumped IPT system is comprised of three components: a power supply, charge-pads and a pick up circuit. A block diagram of the systems is shown in Figure 1. A digital DC power supply is followed by a single-phase square wave inverter operating at 85 kHz. The IPT system consists of resonant compensation networks for the transmitter and receiver coils along with a rectifier followed by a Buck converter in the pick up side. A series-series compensation [9] is considered in this paper. The choice is motivated mainly by the main advantages of series-series compensation technique, for example, independence of the compensation capacitors from the magnetic coupling of the coils and consequently, high tolerance of the system to coil misalignment [14]. A rectifier followed by a DC-DC Buck converter is used in the pick-up circuitry to charge the traction battery.

The specifications of an IPT system typically includes the output power P_2 needed to charge the battery of the traction motor, the frequency of operation, the air gap across which δ the output power must be transferred and maximum dimensions of the coils. The air-gap and the maximum coil dimensions are dependent of the geometrical constraints and cannot be altered during the design process. Based on this an example prototype of an IPT system is shown in Table I. To incorporate the size constraint, maximum dimensions of width and length of the coils are fixed at 200 mm and 220 mm respectively. These constraints are carefully selected considering the air gap of 150 mm to highlight the tradeoffs encountered during charge pad design. Before proceeding to modelling and optimisation, as the next step to design and analysis of IPT system performance the equivalent circuit and modelling the pick up circuit with the load and rectifier.

A. Equivalent Circuit & Load Modelling

Figure 2 shows the equivalent circuit of the magnetically coupled IPT coils which is similar to the equivalent circuit of a transformer model. M denotes the mutual inductance between the two IPT coils and is defined as $M = k\sqrt{L_1 L_2}$, where k is the magnetic coupling co-efficient of the IPT coils and L_1, L_2 are the self-inductances. The value of C_1 and C_2 are chosen to according to series-series compensation topology [9] in order to achieve maximum transmission efficiency.

Based on the analysis presented in [15], the load circuit of

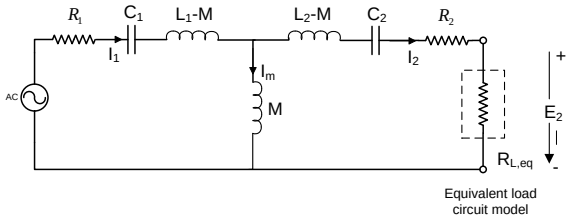

Fig. 2. Equivalent circuit of an IPT system with series-compensated capacitors on the primary and the pick up. $M = k\sqrt{L_1 L_2}$ is the mutual inductance and $(L_1 - M)$, $(L_2 - M)$ are the leakage inductances. Compensating capacitors are $C_1 = \frac{1}{\omega_o^2 L_1}$ and $C_2 = \frac{1}{\omega_o^2 L_2}$. The series resistances of the coils are R_1 and R_2.

the pick-up or receiver side is modelled as an equivalent load resistance of a series-series compensated IPT system as shown in Figure 3. The equivalent load resistance is calculated as:

$$R_{L,eq} = \frac{8}{\pi^2} R_L \tag{1}$$

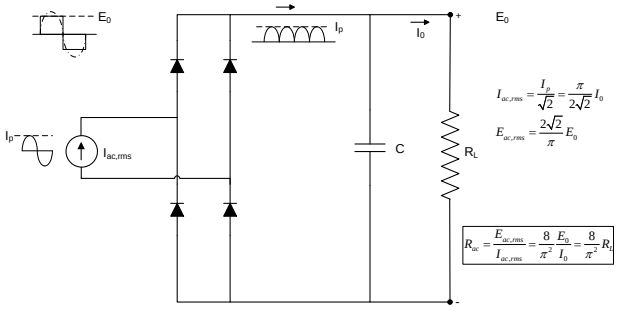

Fig. 3. Equivalent resistance modelling of the rectifier and the load. The load resistance is modelled as $R_L = \frac{U_{2,dc}^2}{P_2}$. The input of the rectifier for series-series compensation is modelled as a current source. I_p is the ac-current induced in the compensated pick up coil. I_o is the rectified output of the sinusoidal current I_p.

B. Power output & Efficiency

The power output of of an IPT system can be quantified as the product of the open circuit voltage V_{oc} and the short circuit current (I_{sc}) and the quality factors ($Q_i = \frac{\omega L_i}{R_i}$) of the charge pads [16]. It can be rewritten in terms of the VA at the input terminals of the transmitter pads, the coupling co-efficient and the operating Q of the receiver circuit (Q_r):

$$P_2 = P_{out} = V_{oc} I_{sc} Q_r = (V_{in} I_1) k^2 Q_r \tag{2}$$

From the above equation, it can be concluded that high values of k are desired so that less MMF will be required to get the same power transfer, therefore leading to lower inverter ratings and sizes. Increasing the operating Q of the receiver circuit is also a good solution but a very high quality can lead to narrow bandwidth leading to tuning problems [17].
As shown in [18], the theoretical maximum transfer efficiency η_{max} of the IPT system can be shown as :

$$\eta_{max} \approx \frac{k^2 Q^2}{(1 + \sqrt{1 + k^2 Q^2})^2} \tag{3}$$

where the inductor quality factor Q is the geometric mean of the two quality factors Q_1 and Q_2. The highest magnetic efficiency arises if the pad losses are equal on the primary and secondary sides. From equation 3, it is quite evident that maximum efficiency is limited by the product of magnetic coupling k and inductor quality factor leading to the terming the product kQ as the Figure of Merit (FOM) of IPT systems.

C. Charge-pad Layout

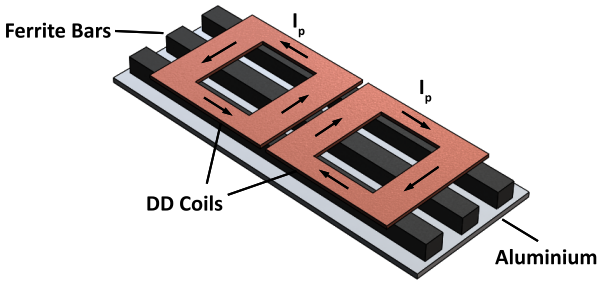

Fig. 4. Layout of primary and secondary DD charge pads. Ferroxcube I-shaped ferrite bars 3C-90 are used to improve magnetic coupling. Aluminium plates are used behind both primary and pick up charge pads (not shown in figure) for shielding purposes.

The coil layout used in this paper as shown in Figure 4 is a polarized single sided charge pad also known as DD coil topology. The main motivation of choosing this coil design is their relatively higher tolerance to misalignment and high fundamental flux path compared to conventional circular pads [16]. To improve magnetic coupling and shaping of the I-shaped field ferrite bars are used below the charge pads. The aluminium (Al) sheet is used to provide structural rigidity to the pad and shields any leakage stray fields generated to satisfy the ICNIRP guidelines of maximum leakage magnetic fields in IPT systems.

III. FE Modelling of IPT Coils

In this section, the theoretical design considerations are taken into account and are extended to detailed 3D FE models for frequency domain analysis. The calculations of the copper losses, core losses and the aluminium losses are discussed here. The FE model built in this section is used for the subsequent $\eta - \alpha - w$ optimisation discussed in Section IV.

A. 3D Finite Element Modelling

A 3D FE model is developed in this section for calculation of the IPT system parameters. Figure 5 shows the sectional 2D plot of the simulation model using commercially available software COMSOL. The litze wire DD winding is modelled as a rectangular multi-turn coil domain in the model with uniform current density in the cross section. This reduces the computational load since the it will not compute the eddy current losses in the winding. This approximations are valid in this model since the litze wire strand diameter is chosen lower than the skin depth of copper at the operating frequency 85 kHz.

To increase the magnetic coupling of the coils, ferrite bars

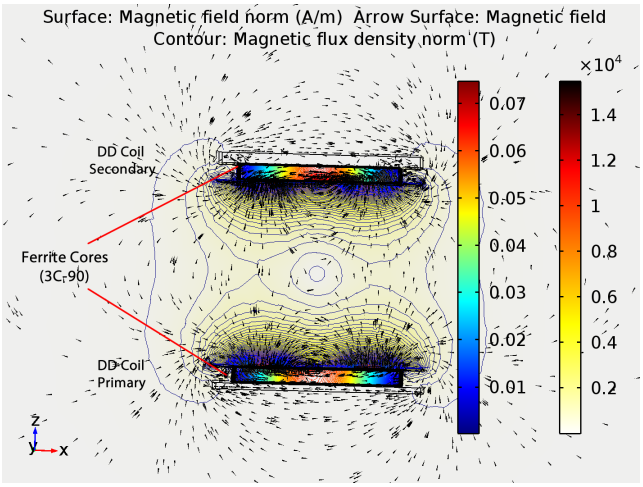

Fig. 5. Plot of magnetic flux density in the simulated model. For better visualization, a section 2-D plot of the 3D model is presented here.

are added to the design as already shown in Figure 5. The core is modelled with a linear or constant relative permeability of $\mu_r = 2400$ to resemble that of material 3C-90. The conductivity of the core material is low ($\sigma = 0.2$ S/m) and therefore eddy currents in the core are neglected unlike the aluminium shields.
The unbounded space around the coils is bounded by a sphere with radius equal to five times the length of the charge pads, so that the accuracy of the simulations is independent of the size of the sphere. Magnetic shielding boundary condition is applied to the bordering surfaces of the sphere. Physics based automated meshing techniques are used to mesh the entire geometry. For accurate computation of the eddy currents and

the stray fields, dense meshing is used in the aluminium shields with a maximum mesh size of one-third of thickness of the aluminium shield.

B. Computation of Losses

The type of losses incurred in the above IPT system are mainly: a) DC copper losses, b) AC losses in litze wire (skin and proximity losses), c) Core losses in ferrite bars and d) Aluminium eddy current losses. Detailed analysis of ac-losses of litze wire winding is not considered in this paper. Therefore, only the dc copper losses are considered.
The core losses are calculated by integrating the core loss density according to the Steinmetz equation:

$$p_{core} = \kappa f_0^{\alpha} \hat{B}^{\beta} \tag{4}$$

over the volume of the ferrite cores. The Steinmetz parameters of the core material 3C-90 are $\kappa = 3.2E-3$, $\alpha = 1.46$ and $\beta = 2.75$.
The skin depth of aluminium at an operating frequency of 85 kHz is 0.28 mm which is quite small compared to the dimensions of the aluminium shields. An Impedance Boundary condition is used in the FE model which essentially sets the skin depth to zero, making all induced currents flow on the surface of the conductors. Mathematically, the relation between the magnetic (**H**) and electric field (**E**) at the boundary reads:

$$\mathbf{n} \times \mathbf{H} + \sqrt{\frac{\epsilon - j\sigma/\omega}{\mu}} \mathbf{n} \times (\mathbf{E} \times \mathbf{n}) = 0 \tag{5}$$

The distribution of the dissipated power, P_d (SI unit: W/m^2) can be calculated from:

$$P_d = \frac{1}{2}(\mathbf{J}_S . \mathbf{E}^*) \tag{6}$$

where $\mathbf{J}_S$ is the induced surface current density, and the asterisk (*) denotes the complex conjugate. The overall aluminium eddy losses (P_{al}) are computed by an area integral of the dissipated power (P_d) over the surface of the aluminium shield.

C. IPT System Analysis

The numerical analysis of IPT is performed by a combination of MATLAB to create and postprocess the FE models and COMSOL to solve the FE models. To save time a minimum number of preferably static simulations is executed and IPT system characteristics are obtained by post-processing the results. The analysis of a single IPT design is comprised of the following steps:

- Simulation of primary and secondary DD coils to determine L_p, R_p and L_s, R_s.
- Simulation of total IPT system with primary excited and secondary open circuited. The open circuit voltage (V_{oc}) is used to compute the mutual inductance $M = \frac{V_{oc}}{j\omega I_p}$ where I_p is the primary current.
- Computation of coupling co-efficient k using the formula $k = \frac{M}{\sqrt{L_p L_s}}$.
- Circuit simulation using $L_p, R_p, L_s, R_s, M, Z_{load}$ to extract primary current based on a fixed load or secondary current.
- Simulation of IPT system with primary and secondary both excited to extract magnetic stray fields, copper losses (P_{cu}), core (P_{core}) and aluminium eddy losses (P_{al}).
- Calculation of overall transfer efficiency of the IPT system, $\eta = \frac{P_{out}}{P_{out}+P_{core}+P_{cu}+P_{al}}$.

IV. $\eta - \alpha - w$ Optimisation

A comparison between IPT design types is only fair if the designs under consideration are designed optimally for the requirements, so an optimisation approach is required. Any engineering related optimisation approach consists of two parts: models to describe the problem and an algorithm to control the optimisation. The models used here are all based on 3D FE computations, which allows a simple comparison of completely different IPT system designs. Non-linearity of ferrite cores can also be taken into account, however the flux levels seen from preliminary investigation shows the operating values are well below the saturation limit of the ferrite material used.

A. Particle Swarm Optimisation

The optimisation algorithm used is particle swarm algorithm, an evolutionary gradient free method based on the movement of birds or insects in a swarm. This algorithm was selected because it is gradient free and potentially requires very few function calls [19].
1) Multi-Objective PSO: A modified version of the original algorithm is used here to work with multiple targets simultaneously, which allows the pareto optimal fronts [11] to be computed. This is accomplished by storing all pareto optimal solutions in a repository and picking the global best target randomly from this repository.
2) Solution Space and Constraint handling: To prevent unnecessary exploration of uninteresting design regions and save computing time, the global targets are confined to more promising parts of the solution space, such as high efficiency or low weight designs. To ensure variable values within constraints, velocity reduction techniques on particles are used.

B. Optimisation Targets, Variables, Constraints

The setup of the optimisation consists of specifying variables, constants, constraints and targets. Considering a theoretical 1-kW, 15 cm air-gap lumped IPT system for dynamic charging of EVs, the following global optimisation targets are chosen:

- Maximize power transfer efficiency
- Maximize area-power density of EV pick up
- Minimize active weight of the IPT charge pads

Figure 6 shows the major design variables. The optimisation variables are all geometrical in nature and their ranges are presented in Table II. The effect of the chosen variables on the magnetic properties of the IPT systems are briefly discussed here. The number of turns (N) of the coils is an important

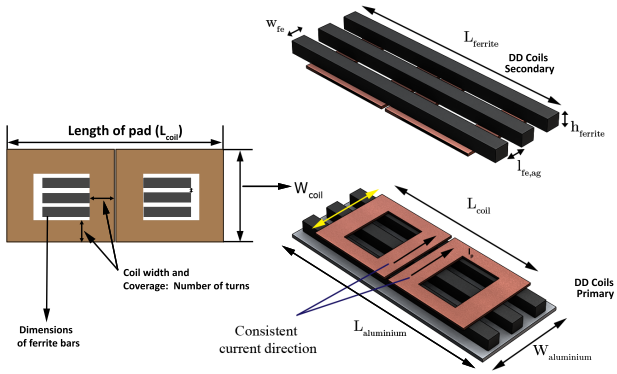

Fig. 6. Graphical representation of optimisation variables. Inter-ferrite relative airgap is defined as $p_{ag} = \frac{l_{fe,ag}}{(W_{coil}/2 - w_{fe})}$. Relative length of ferrites is defined as $p_{fe} = \frac{L_{fe}}{L_{coil}}$. Number of turns in the coil layout determines the coil coverage or the coil width as shown in the figure.

TABLE II
RANGE OF OPTIMISATION VARIABLES

Variables	Expression	Range
Number of turns	N	$15 \leq N \leq 40$
Number of ferrites	n	3
Width of ferrites (mm)	w_{fe}	$10 \leq w_{fe} \leq 25$
Thickness of ferrites (mm)	h_{fe}	$5 \leq h_{fe} \leq 12$
Inter-ferrite relative air-gap (%)	p_{ag}	$0 \leq p_{ag} \leq 60$
Relative length of ferrites (%)	p_{fe}	$50 \leq p_{ag} \leq 100$
Thickness of aluminium (mm)	t_{al}	$5 \leq t_{al} \leq 10$

design variable since the resistance, inductance and coil coverage is dependent on that. The choice of ferrite dimensions and optimal placement strategy is an interesting study undertaken in this research. To the best knowledge of the authors, there is not sufficient literature about the effect of ferrite dimensions and placement on IPT performance. Figure 7 presents the results of the variation of coupling co-efficient with ferrite length and airgap between the bars. Stray or leakage fluxes around the coil region are dependent on the thickness of the aluminium used and also on the positioning of the ferrite cores as shown in Figure 8. To ensure that the optimisation does not lead to unrealistic designs in terms of thermal management, there are limits put on the primary current (25 A) and the flux density in the cores ($\leq B_{sat} = 0.45T$). To abide by the ICNIRP guidelines, an upper limit on the stray field (27 μT at a radial distance of 300 mm from back-end of the charge pads) is imposed.

C. Results of Optimisation

The results obtained from optimization should be carefully analysed before drawing scientific conclusions based on it. The optimization procedure generates a lot of data and a significant time must be devoted into post-processing those results to investigate possibilities of errors. Errors in IPT models can lead the optimization algorithm in to solving an entirely different problem leading to erroneous results. Fig. 10 and

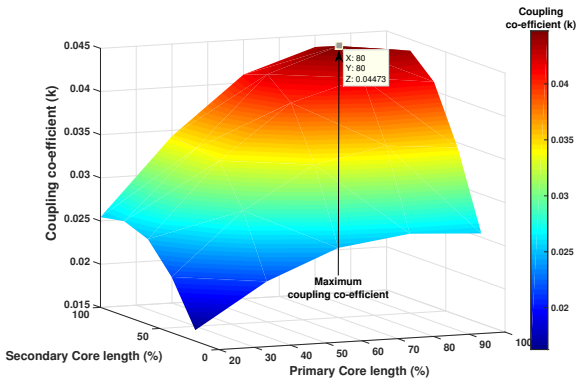

(a) Variation of coupling co-efficient with length of ferrite bars

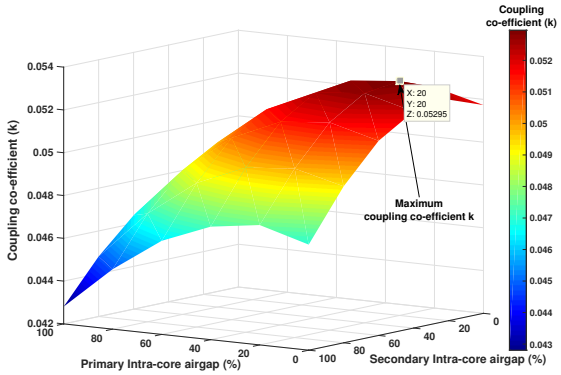

(b) Variation of coupling co-efficient with air-gap between ferrite bars

Fig. 7. Effect of ferrite dimensions and placement strategy on coupling co-efficient k between the charge pads. The results show that the coupling is maximum when the length of ferrites is 80% of the charge pad length and the percentage airgap (p_{ag}) is 20% when used with 3 ferrite bars.

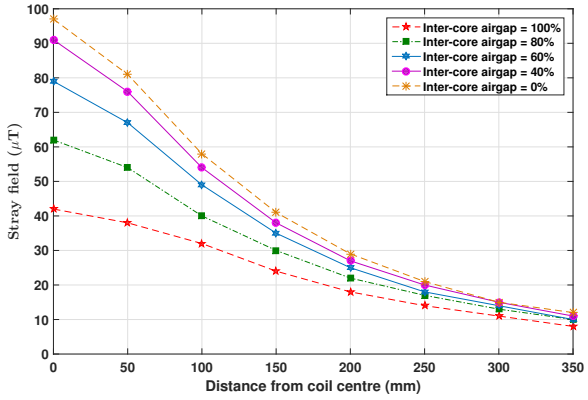

Fig. 8. Graphical representation of the decay of the stray field (μT) from the charge pads at different placement strategies of the ferrite core. Thickness of aluminium shield (t_{al}) is 3 mm.

Fig. 11 shows the 2D pareto fronts of the global optimisation targets. To gain more insight into the optimization process some secondary plots derived from the main pareto fronts will also be presented in Fig 12 and 13. After careful consideration of the results the following observations are made:

- Fig. 10 shows the plot of maximum power transfer effi-

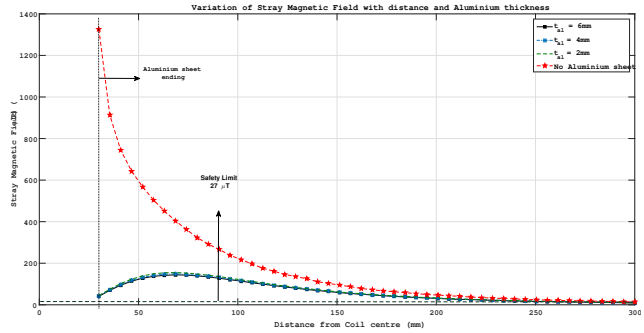

Fig. 9. Graphical representation of the decay of the stray field (μT) from the charge pads at different placement strategies of the ferrite core. Thickness of aluminium shield (t_{al}) is 3 mm.

ciency of the optimal IPT designs with the active weight of the design. The trend shows increasing efficiency with heavier designs. It can be explained by increased weight of copper (higher number of turns) and ferrite bars leading to higher coupling co-efficient (k) and quality factor (Q) of the coils. This can be verified with plot of FOM (kQ) with weight in Fig. 12.

- Fig. 11 shows the pareto plot of the power transfer efficiency with area-related power efficiency of the secondary or the pick up coil. With higher power density or with lower area coverage of the coils, mutual inductance between the coils decreases leading to lower coupling factors leading to low efficiencies.
- Fig. 13 presents the trend in the IPT losses. It is seen that the core losses are quite negligible compared to the copper and the aluminium losses. In light and small designs, the coupling co-efficient and the charge pad quality factors are too low leading to higher primary currents to transfer the same amount of power, thus increasing the losses in the system.

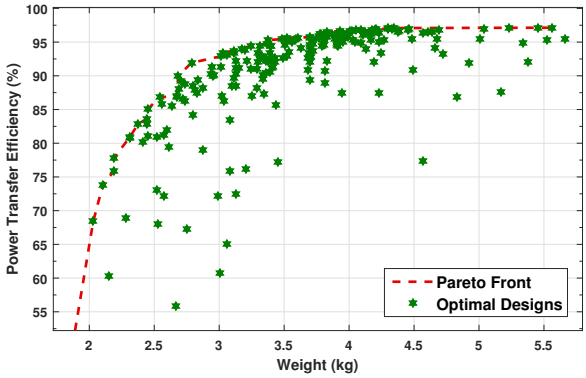

Fig. 10. Plot of maximum efficiency versus system weight of the IPT system. The trend shows higher efficiencies with increasing weight of the designs. Due to increased copper weight mainly because of higher number of turns and increased ferrite weight leads to higher magnetic coupling and higher quality factors which in turn increases efficiency.

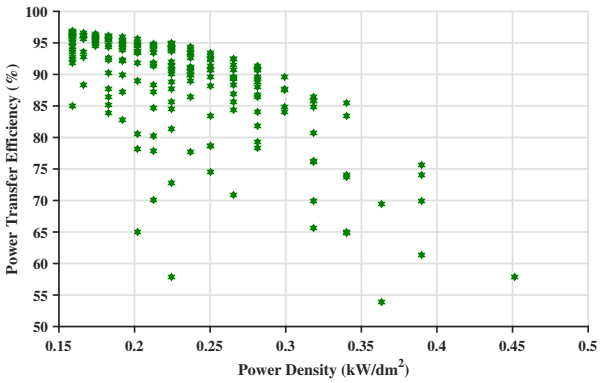

Fig. 11. $\eta - \alpha$ Pareto front of optimal designs. The trend shows decreasing efficiencies with increasing area-power density of the designs.

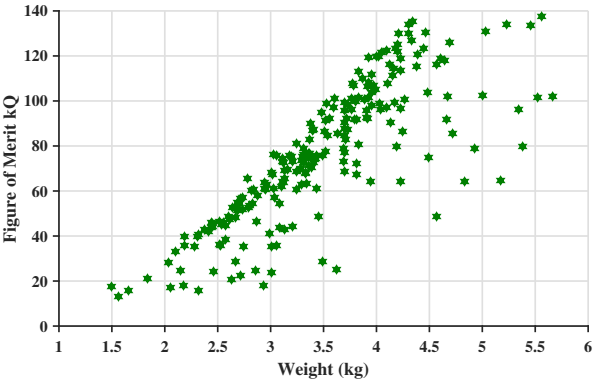

Fig. 12. Plot of FOM of optimal IPT designs versus weight of IPT system. With heavier designs the coupling co-efficient and quality factor of the coils increase leading to higher FOM (kQ). This leads to higher efficiencies in heavier designs.

V. Experimental Verification

In this section, the 3D modelling procedure discussed in Section III will be validated using experimental results.In this paper, a co-planar DD coil configuration is considered for FE modelling and further optimisation. However, for experimental validation instead of a DD configuration, a square coil shape with core as both primary and secondary pick up is used. The geometrical layout remains the same as that of DD coil configuration. Details of the coils are presented in Table III. The self-inductance of the coils as measured by an LCR meter

TABLE III
Design Details of the Experimental Setup

Variables	Value	Description
N_p	26	Primary number of turns
N_s	16	Secondary number of turns
r_w	1.2 mm	Radius of litze wire
$L_p \times W_p$	20 cm×20 cm	Dimensions of primary coil
$L_s \times W_s$	10 cm×10 cm	Dimensions of secondary coil
w_{core}	3 mm	Width of core
h_{core}	2.75 mm	Height or thickness of core
z_{ag}	20 mm	Airgap between coils

are 117 μH and 16 μH respectively, which are quite close to

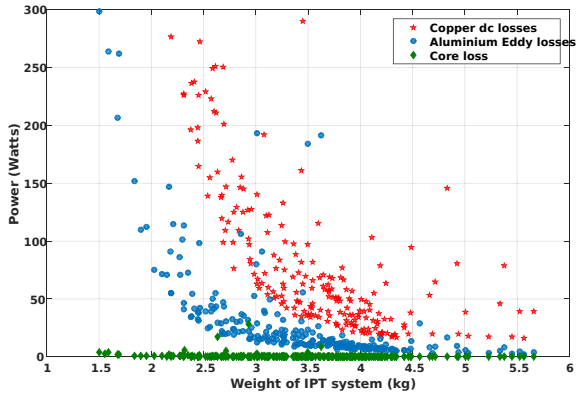

Fig. 13. Distribution and variation of system losses with weight of optimal designs. Core losses are comparatively negligible to copper and aluminium losses. The reduction of the losses in heavier designs is mainly due to high primary currents required to compensate for lower coupling in lighter designs.

the FE results, 111 μH and 15.2 μH. The comparative results of coupling of the two coils with presence or absence of cores and placement strategy of the ferrite bars are shown in Fig. 14.

The above graphs show good agreement between them with percentage error ranging from 1-4 % approximately, thus validating the model.

VI. Conclusion

In this paper, the framework for a multi-objective optimisation of a 1-kW, 15 cm airgap IPT system is presented. The FE modelling procedure is discussed in detail and experimentally verified. The optimisation targets, variables and constraints are chosen with detailed justification. From the results of the simulation it is seen that the dimensions,positioning of the ferrite cores with respect to each other influence the magnetic behaviour of the IPT system. It is seen that with decreasing airgap between cores results in an increase of mutual inductance and coupling co-efficient of the IPT coil systems at the cost of increasing stray fields. Trade-offs encountered in the $\eta-\alpha-w$ optimisation are discussed in detail with design guidelines showing the conditions to increase power transfer efficiency. Thermal management of IPT systems is not considered in this paper. Future research, can, therefore address an optimisation of a system with detailed loss analysis coupled with integrated thermal model to determine the electro-thermal performance of high power IPT systems.

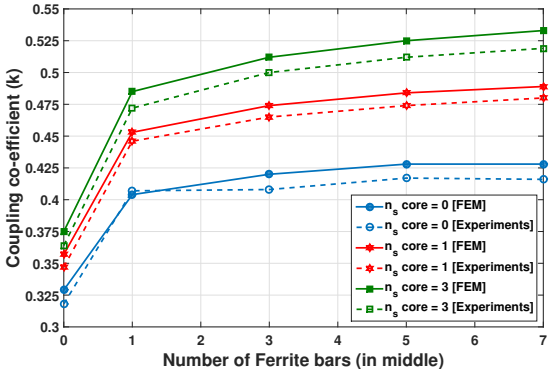

(a) Variation of coupling co-efficient with number of ferrite bars used in the charge pads.

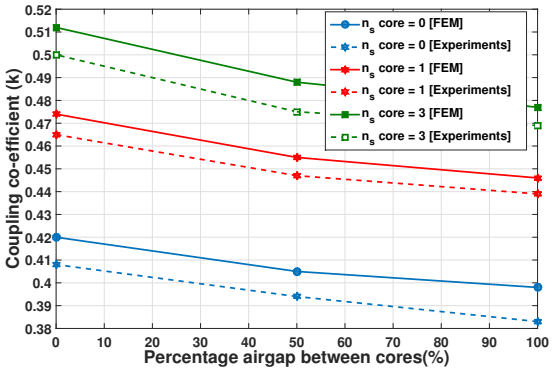

(b) Variation of coupling co-efficient with air-gap between ferrite bars ($n_{fe} = 3$).

Fig. 14. Effect of number of ferrites and placement strategy on coupling co-efficient k between the charge pads. The above figures show good accordance between results obtained from the FE model and the experiments. The maximum error is 4%.

References

[1] K. Knaisch and P. Gratzfeld, "Comparison of Magnetic Couplers for Inductive Electric Vehicle Charging Using Accurate Numerical Simulation and Statistical Methods," 2015.

[2] G. Covic and J. Boys, "Inductive Power Transfer," *Proceedings of the IEEE*, vol. 101, no. 6, pp. 1276–1289, 2013.

[3] X. Mou and H. Sun, "Wireless power transfer: Survey and roadmap," *IEEE Vehicular Technology Conference*, vol. 2015, no. 646470, pp. 1–13, 2015.

[4] M. Eghtesadi, "Inductive power transfer to an electric vehicle-analytical model," *40th IEEE Conference on Vehicular Technology*, pp. 100–104, 1990.

[5] A. Shekhar, V. Prasanth, P. Bauer, and M. Bolech, "Economic Viability Study of an On-Road Wireless Charging System with a Generic Driving Range Estimation Method," *Energies*, vol. 9, no. 2, p. 76, 2016.

[6] V. Prasanth and P. Bauer, "Distributed IPT systems for dynamic powering: Misalignment analysis," *IEEE Transactions on Industrial Electronics*, vol. 61, no. 11, pp. 6013–6021, 2014.

[7] C. Power, T. a. Case, S. Chopra, P. Bauer, and S. Member, "Driving Range Extension of EV with On-road," vol. 60, no. c, pp. 1–11, 2011.

[8] International Commission on Non-Ionizing Radiation Protection (ICNIRP), "Guidelines for limiting exposure to time-varying electric, magnetic, and electromagnetic fields (up to 300 GHz)," *Health Physics*, vol. 74, no. 4, 1998.

[9] E. Waffenschmidt and T. Staring, "Limitation of inductive power transfer for consumer applications," *Power Electronics and Applications, 2009. EPE '09. 13th European Conference on*, pp. 1–10, 2009.

[10] M. van der Geest, H. Polinder, and J. a. Ferreira, "Optimization and comparison of electrical machines using particle swarm optimization," *XXth ICEM*, 2012.

[11] C. a. C. Coello, G. T. Pulido, and M. S. Lechuga, "Handling multiple objectives with particle swarm optimization," *Evolutionary Computation, IEEE Transactions on*, vol. 8, no. 3, pp. 256–279, 2004.

[12] R. Bosshard, J. W. Kolar, J. Muehlethaler, I. Stevanovic, B. Wunsch, and F. Canales, "Modeling and Pareto Optimization of Inductive Power Transfer Coils for Electric Vehicles," *Emerging and Selected Topics in Power Electronics, IEEE Journal of*, vol. PP, no. 99, p. 1, 2014.

[13] G. a. Covic, M. L. G. Kissin, D. Kacprzak, N. Clausen, and H. Hao, "A bipolar primary pad topology for EV stationary charging and highway power by inductive coupling," *IEEE Energy Conversion Congress and*

Exposition: Energy Conversion Innovation for a Clean Energy Future, ECCE 2011, Proceedings, pp. 1832–1838, 2011.

[14] R. Bosshard, J. W. Kolar, and B. Wunsch, "Accurate finite-element modeling and experimental verification of inductive power transfer coil design," *2014 IEEE Applied Power Electronics Conference and Exposition - APEC 2014*, pp. 1648–1653, 2014.

[15] R. L. Steigerwald, "Comparison of Half-Bridge Resonant Converter Topologies.," *IEEE Transactions on Power Electronics*, vol. 3, no. 2, pp. 174–182, 1988.

[16] M. Budhia and J. Boys, "Development of a single-sided flux magnetic coupler for electric vehicle IPT charging systems," *..., IEEE Transactions on*, vol. 60, no. 1, pp. 318–328, 2013.

[17] G. A. Covic, S. Member, and J. T. Boys, "Modern Trends in Inductive Power Transfer for Transportation Applications," vol. 1, no. 1, pp. 28–41, 2013.

[18] K. Van Schuylenbergh and R. Puers, *Inductive Powering: Basic Theory and Application*, vol. 151. 2009.

[19] Y. Duan and R. G. Harley, "A Novel Method for Multiobjective Design and Optimization of Three Phase Induction Machines," *IEEE Transactions on Industry Applications*, vol. 47, pp. 1707–1715, July 2011.